Int J Thermophys (2009) 30:1697–1723
DOI 10.1007/s10765-009-0638-7

Disturbance due to Thermal and Mass Loads in Generalized Elasto-thermodiffusive Solids

J. N. Sharma · Nisha Kumari · K. K. Sharma

Received: 11 November 2008 / Accepted: 3 August 2009 / Published online: 2 September 2009

Abstract The one-dimensional problem of a generalized elasto-thermodiffusive solid half-space, whose surface is maintained traction free but subjected to the action of thermal or mass concentration loads, has been investigated. The model, composed of basic governing equations and boundary conditions, has been solved by using the Laplace transform technique. As we know that the 'second sound' effects are short lived, thus, short-time approximations of solutions for dilatation, chemical potential, and stress functions have been obtained. The short-time solutions for each considered function consist of three waves, namely, elasto-diffusive, mass-diffusive, and thermo-diffusive waves traveling with distinct speeds. The discontinuities at the wave fronts of various considered physical quantities have also been discussed. To obtain the dilatation, chemical potential, and stress in the physical domain due to instantaneous, continuous, and periodic loads, the transformed solutions of these functions have been inverted by employing a numerical technique. Finally, the dilatation, chemical potential, and stress functions have been computed numerically for copper and brass materials. The computer-simulated results so obtained have been presented graphically to illustrate the analytical developments.

Keywords Diffusion · Laplace transform · Second sound · Thermal and mass concentration loads · Wave front

J. N. Sharma (✉) · N. Kumari · K. K. Sharma
Department of Applied Sciences and Humanities, National Institute of Technology-Hamirpur, Hamirpur 177005, India
e-mail: jns@nitham.ac.in

N. Kumari
e-mail: nishanit@yahoo.co.in

K. K. Sharma
e-mail: kks@nitham.ac.in

1 Introduction

Biot [1] developed the coupled theory of thermoelasticity to eliminate the paradox inherent in the classical uncoupled theory that elastic changes have no effect on the temperature. The heat equations for both theories, however, are of the diffusion type, predicting an infinite speed of propagation. To account for the finite speed of wave propagation, Lord and Shulman [2] developed the theory of generalized thermoelasticity with one relaxation time included in the classical Fourier law of heat conduction. The heat equation associated with this theory is of the wave type which ensures a finite speed of wave propagation of heat and elastic waves. The governing equation of motion and constitutive relations remains the same as those for coupled and uncoupled theories of thermoelasticity. Nowacki [3–6] developed the theory of thermoelastic diffusion by using the coupled thermoelastic model. Dudziak and Kowalski [7] and Olesiak and Pyryev [8], respectively, discussed the theory of thermodiffusion and the influence of cross effects arising due to coupling in the fields of temperature, mass diffusion, and strain in an elastic cylinder. Danilovskaya [9,10] treated the problems of thermal shock on the surface of a half-space for the first time and obtained its analytical solution in dynamic uncoupled thermoelasticity. Nayfeh [11] considered the transient response of thermoelastic waves in a half-space and observed a strong coupling effect between thermal and dilatation motion as well as the presence of a thermal damping term which makes a short-time solution meaningful. Song et al. [12] studied transient waves caused by a line heat source moving with a uniform velocity inside a homogeneous isotropic thermoelastic half-space under the Green–Lindsay (G–L) model of generalized thermoelasticity.

Sherief et al. [13] derived the basic governing equations of motion, heat conduction, and mass diffusion for a generalized elasto-thermodiffusive solid. Sherief and Helamy [14] investigated the problem of a half-space whose surface is rigidly fixed and subjected to the action of thermal shock in the context of the generalized theory of thermoelasticity. Sherief and Saleh [15] studied the half-space problem in the context of generalized thermoelastic diffusion when the surface of the half-space is assumed traction free and subjected to a time-dependent thermal shock. Sharma [16] discussed the propagation of plane harmonic waves in generalized thermoelastic diffusive heat conducting solids. Sharma et al. [17] have also studied the propagation of surface waves in a generalized elasto-thermodiffusive half-space. Assuming that the disturbance is harmonically time dependent, Sharma et al. [18,19] have obtained a general solution to the field equations of homogeneous isotropic, generalized thermoelastic diffusion with two relaxation times using Fourier transforms.

In this article, an attempt has been made to study the propagation of a disturbance in an elasto-thermodiffusive solid half-space when thermal and mass concentration loads are acting on its boundary. Analytical expressions of various physical quantities are obtained at small times. The Laplace transform has been inverted numerically to obtain the considered field functions in the physical domain, in the general case. The analytical developments have also been illustrated numerically and are presented graphically.

2 Basic Equations

The basic governing equations and constitutive relations for the generalized thermodiffusive interactions in a homogeneous isotropic, elastic solid are [13] outlined below:

1. Strain–displacement relations

$$e_{ij} = \frac{1}{2}\left(u_{i,j} + u_{j,i}\right); \quad i, j = 1, 2, 3 \tag{1}$$

2. Stress–strain–temperature–concentration relations

$$\sigma_{ij} = \lambda e_{kk}\delta_{ij} + 2\mu e_{ij} - \beta_1 T\delta_{ij} - \beta_2 C\delta_{ij,} \tag{2}$$

$$\rho T_0 S = \rho C_e T + \beta_1 T_0 e_{kk} + aT_0 C \tag{3}$$

$$P = -\beta_2 e_{kk} + bC - aT; \quad i, j, k = 1, 2, 3 \tag{4}$$

These equations are also known as constitutive relations.

3. Equations of motion

$$\mu u_{i,jj} + (\lambda + \mu)u_{j,ij} - \beta_1 T_{,i} - \beta_2 C_{,i} + \rho F_i = \rho\ddot{u}_i; \quad i, j = 1, 2, 3 \tag{5}$$

4. Equation of heat conduction

$$KT_{,ii} - \rho C_e(\dot{T} + t_0\ddot{T}) = \beta_1 T_0(\dot{e} + t_0\ddot{e}) + aT_0(\dot{C} + t_0\ddot{C}); \quad i = 1, 2, 3 \tag{6}$$

5. Equation of mass diffusion

$$C_{,ii} - \frac{1}{Db}(\dot{C} + t_1\ddot{C}) = \frac{\beta_2}{b}e_{,ii} + \frac{a}{b}T_{,ii}; \quad i = 1, 2, 3 \tag{7}$$

where $\beta_1 = (3\lambda + 2\mu)\alpha_T$, $\beta_2 = (3\lambda + 2\mu)\alpha_C$, e is the dilatation; λ and μ are Lamé parameters; α_T is the coefficient of linear thermal expansion, α_C is the coefficient of linear diffusion expansion, ρ is the density; C_e is the specific heat at constant strain, a is the thermo-diffusive constant, b is the diffusive constant, K is the thermal conductivity, P is the chemical potential per unit mass, T is the absolute temperature, C is the concentration, T_0 is the uniform reference temperature assumed to obey the inequality $|(T - T_0)/T_0| \ll 1$, t_0 and t_1 are thermal relaxation time parameters, and u_i's ($i = 1, 2, 3$) are the displacement components. Here, the comma notation is used for space derivatives and superposed dots denote time differentiation. We assume that material parameters satisfy the inequalities,

$$K > 0, \quad D > 0, \quad \lambda > 0, \quad \rho > 0, \quad C_e > 0, \quad \mu > 0, \quad T_0 > 0, \quad t_0 > 0, \quad t_1 > 0 \tag{8}$$

3 Formulation of the Problem

We consider a homogeneous isotropic, thermodiffusive, elastic solid half-space at a uniform temperature T_0 and initial concentration C_0 in the undisturbed state. We take the origin of the Cartesian coordinate system $O - xyz$ at any point on the surface of the solid and choose the x-axis in such a way that the half-space is represented by $x \geq 0$. From symmetry considerations, we assume that all physical quantities are functions of x and t only. The upper surface of the half-space ($x \geq 0$) is subjected to a time-dependent thermal or mass concentration load. All the field functions are assumed to be bounded and vanish as $x \to \infty$. Equations 5–7 of linear generalized elasto-thermodiffusion governing the displacement $u(x,t)$, temperature $T(x,t)$, and concentration $C(x,t)$, in the absence of body forces and heat sources, become

$$\begin{aligned}(\lambda+2\mu)u_{,xx} - \beta_1 T_{,x} - \beta_2 C_{,x} &= \rho\ddot{u}\\ KT_{,xx} - \rho C_e(\dot{T} + t_0\ddot{T}) &= \beta_1 T_0(\dot{u}_{,x} + t_0\ddot{u}_{,x}) + aT_0(\dot{C} + t_0\ddot{C})\\ C_{,xx} - \frac{1}{Db}(\dot{C} + t_1\ddot{C}) &= \frac{\beta_2}{b}u_{,xxx} + \frac{a}{b}T_{,xx}\end{aligned} \tag{9}$$

Equations 2–4 in the instant case provide us with

$$\begin{aligned}\sigma_{xx} &= (\lambda+2\mu)u_{,x} - \beta_1 T - \beta_2 C\\ P &= -\beta_2 u_{,x} + bC - aT\\ T &= \frac{T_0 S}{C_e} - \frac{\beta_1 T_0}{\rho C_e}u_{,x} + \frac{aT_0 C}{\rho C_e}\end{aligned} \tag{10}$$

where $\vec{u}(x,t) = (u,0,0)$, $T(x,t)$, and $C(x,t)$ are, respectively, the displacement vector, temperature deviation, and concentration change of the material. To facilitate the solution, we define the following quantities:

$$\begin{aligned}&x' = \frac{\omega^* x}{c_L},\quad u_i' = \frac{\rho\omega^* c_L u_i}{\beta_1 T_0},\quad T' = \frac{T}{T_0},\quad C' = \frac{C}{C_0},\quad t_0' = \omega^* t_0,\quad t_1' = \omega^* t_1,\\ &t' = \omega^* t,\quad c_s^2 = \frac{\mu}{\rho},\quad \omega^* = \frac{C_e(\lambda+2\mu)}{K},\quad \varepsilon_T = \frac{T_0\beta_1^2}{\rho C_e(\lambda+2\mu)}, \delta^2 = \frac{c_{\mathrm{s}}^2}{c_{\mathrm{L}}^2},\\ &\bar{a} = \frac{aC_0}{\rho C_e},\quad \bar{\beta} = \frac{\beta_2 C_0}{\beta_1 T_0},\quad \bar{b} = \frac{aT_0}{bC_0},\quad \bar{\omega}_b = \frac{c_{\mathrm{L}}^2}{\omega^* Db},\quad \varepsilon_{\mathrm{C}} = \frac{\beta_1\beta_2 T_0}{C_0 b(\lambda+2\mu)},\\ &c_{\mathrm{L}}^2 = \frac{(\lambda+2\mu)}{\rho},\quad \sigma_{xx}' = \frac{\sigma_{xx}}{\beta_1 T_0},\quad P' = \frac{P}{bC_0},\quad S' = \frac{S}{C_e}\end{aligned} \tag{11}$$

Upon introducing the quantities in Eq. 11 in Eqs. 9 and 10, we obtain

$$\vec{u}_{,xx} - T_{,x} - \bar{\beta}C_{,x} = \ddot{\vec{u}} \tag{12}$$

$$T_{,xx} - (\dot{T} + t_0\ddot{T}) - \varepsilon_T(\dot{u}_{,x} + t_0\ddot{u}_{,xx}) - \bar{a}(\dot{C} + t_0\ddot{C}) = 0 \tag{13}$$

$$C_{,xx} - \bar{\omega}_b(\dot{C} + t_1\ddot{C}) - \varepsilon_{\mathrm{C}}u_{,xxx} - \bar{b}T_{,xx} = 0 \tag{14}$$

$$\begin{aligned} \sigma_{xx} &= u_{,x} - T - \bar{\beta} C \\ P &= -\varepsilon_{\mathrm{C}} u_{,x} + C - \bar{b} T \\ T &= S + \varepsilon_T u_{,x} + \bar{a} C \end{aligned} \tag{15}$$

where the primes have been suppressed for convenience.

3.1 Initial, Regularity, and Boundary Conditions

The half-space is assumed to be undeformed and at rest as well as at a uniform initial temperature T_0. This leads to the following initial and regularity conditions,

$$\begin{aligned} &u(x,0) = 0 = \dot{u}(x,0), \quad T(x,0) = 0 = \dot{T}(x,0), \quad C(x,0) = 0 = \dot{C}(x,0) \ \text{ for all } x \\ &u(x,t), \quad T(x,t), \quad C(x,t) \to 0 \ \text{ as } \ x \to \infty, \quad \text{for all } t. \end{aligned} \tag{16}$$

The following two sets of boundary conditions on the surface $x = 0$ of the half-space are assumed to be satisfied.

3.1.1 Thermal Loads

The boundary $x = 0$ of the half-space is assumed to be stress free, iso-concentrated, and subjected to a time varying temperature input (TI) or temperature gradient (TG). This leads to

$$\begin{aligned} &\sigma_{xx} = 0, \quad T = \theta_0 f(t), \quad C = 0, \quad \text{for TI} \\ \text{or} \quad &\sigma_{xx} = 0, \quad T_{,x} = -\theta_0 f(t), \quad C = 0, \quad \text{for TG} \end{aligned} \tag{17}$$

3.1.2 Mass Concentration Loads

The surface $x = 0$ of the half-space is assumed to be stress free, isothermal, and subjected to a time varying concentration change (CI) or concentration gradient (CG). This implies that

$$\begin{aligned} &\sigma_{xx} = 0, \quad T = 0, \quad C = C_0 f(t), \quad \text{for CI} \\ \text{or} \quad &\sigma_{xx} = 0, \quad T = 0, \quad C_{,x} = -C_0 f(t), \quad \text{for CG} \end{aligned} \tag{18}$$

Here, $f(t)$ is a well-behaved function of time.

4 Formal Solution of the Problem

Applying the Laplace transform defined by

$$\bar{g}(x, p) = \int_0^\infty g(x,t) \mathrm{e}^{-pt} \mathrm{d}t \tag{19}$$

with respect to time to Eqs. 12–14, we obtain

$$\begin{aligned}(D^2 - p^2)\bar{u} - D\bar{T} - \bar{\beta}D\bar{C} &= 0\\ (D^2 - \tau_0 p^2)\bar{T} - \varepsilon_T \tau_0 p^2 D\bar{u} - \bar{a}\tau_0 p^2 \bar{C} &= 0\\ (D^2 - \bar{\omega}_b p^2 \tau_1)\bar{C} - \varepsilon_C D^3 \bar{u} - \bar{b}D^2\bar{T} &= 0\end{aligned} \tag{20}$$

where $\tau_0 = t_0 + p^{-1}$ and $\tau_1 = t_1 + p^{-1}$.

Solving the system of Eq. 20 and using the regularity conditions, Eq. 16, we get

$$\begin{aligned}\bar{u}(x, p) &= \sum_{i=1}^{3} B_i \mathrm{e}^{-\lambda_i p x}\\ \bar{T} &= \sum_{i=1}^{3} \frac{p}{\lambda_i}\bar{S}_i B_i \mathrm{e}^{-\lambda_i p x}\\ \bar{C} &= \sum_{i=1}^{3} p\lambda_i \bar{W}_i B_i \mathrm{e}^{-\lambda_i p x}\end{aligned} \tag{21}$$

where

$$\bar{W}_i = \frac{\bar{b}\left\{1 - \lambda_i^2(1 + \varepsilon_a)\right\}}{\lambda_i^2(1 + \bar{\beta}\bar{b}) - \bar{\omega}_b\tau_1}, \quad \bar{S}_i = \left\{1 - \lambda_i^2(1 + \bar{\beta}\bar{W}_i)\right\}, \quad i = 1, 2, 3 \tag{22}$$

Here, the quantities $\lambda_i^2 (i = 1, 2, 3)$ are the roots of the equation,

$$\lambda^6 - p^2 A^* \lambda^4 + p^4 B^* \lambda^2 - p^6 C^* = 0 \tag{23}$$

where

$$\begin{aligned}\varepsilon_a &= \frac{\varepsilon_C}{\bar{b}}\\ A^* &= \frac{1 + \bar{\omega}_b\tau_1 + \tau_0\left\{(1 + \bar{a}\bar{b})\,(1 + \varepsilon_a) + (1 + \bar{\beta}\bar{b})(\varepsilon_T - \varepsilon_a)\right\}}{1 - \bar{\beta}\varepsilon_C}\\ B^* &= \frac{\tau_0(1 + \bar{a}\bar{b}) + \bar{\omega}_b\tau_1\{1 + t_0(1 + \varepsilon_T)\}}{1 - \bar{\beta}\varepsilon_C}\\ C^* &= \frac{\bar{\omega}_b\tau_1\tau_0}{1 - \bar{\beta}\varepsilon_C}\end{aligned} \tag{24}$$

Upon applying the Laplace transform to Eq. 15 and using the solution, Eq. 21, the expressions for stress and chemical potential can be obtained as

$$\hat{\sigma}_{xx} = -p\sum_{i=1}^{3} \frac{B_i \mathrm{e}^{-p\lambda_i x}}{\lambda_i}$$

$$\bar{P} = \bar{\omega}_b \tau_1 p \sum_{i=1}^{3} \frac{\bar{W}_i B_i}{\lambda_i} \mathrm{e}^{-p\lambda_i x} \tag{25}$$

The deformation given by $e = \frac{\partial u}{\partial x}$, on applying the Laplace transform with the help of the solution, Eq. 21, leads to

$$\bar{e} = -p \sum_{i=1}^{3} B_i \lambda_i \mathrm{e}^{-\lambda_i p x} \tag{26}$$

4.1 Thermal Loads

Upon applying an integral transform to the boundary conditions, Eq. 17, and using the formal solution, Eq. 21, we obtain a system of three coupled equations in three unknowns $B_i (i = 1, 2, 3)$ as follows:

$$\begin{aligned}
&\lambda_2\lambda_3 B_1 + \lambda_1\lambda_3 B_2 + \lambda_1\lambda_2 B_3 = 0 \\
&\lambda_2\lambda_3 \left(\lambda_1 - \frac{h_T}{p}\right) \bar{S}_1 B_1 + \lambda_1\lambda_3 \left(\lambda_2 - \frac{h_T}{p}\right) \bar{S}_2 B_2 + \lambda_1\lambda_2 \left(\lambda_3 - \frac{h_T}{p}\right) \bar{S}_3 B_3 \\
&\quad = -\frac{\theta_0 f\,(p)}{p^2} \lambda_1\lambda_2\lambda_3 \\
&\bar{W}_1\lambda_1 B_1 + \bar{W}_2\lambda_2 B_2 + \bar{W}_3\lambda_3 B_3 = 0
\end{aligned} \tag{27}$$

Solving the above system of equations, Eq. 27, we obtain

$$B_i = \frac{\theta_0 \bar{f}(p) D_i}{pD}, \quad i = 1, 2, 3 \tag{28}$$

where

$$\begin{aligned}
D &= \begin{cases} pD_{\mathrm{TG}}, & \text{for TG} \\ D_{\mathrm{TI},} & \text{for TI} \end{cases} \\
D_1 &= \lambda_1 \left(\bar{W}_2\lambda_2^2 - \bar{W}_3\lambda_3^2\right), \quad D_2 = \lambda_2 \left(\bar{W}_3\lambda_3^2 - \bar{W}_1\lambda_1^2\right), \\
D_3 &= \lambda_3 \left(\bar{W}_1\lambda_1^2 - \bar{W}_2\lambda_2^2\right)
\end{aligned} \tag{29}$$

Here,

$$\begin{aligned}
D_{\mathrm{TG}} &= \left[\bar{S}_1\lambda_1 \left(\bar{W}_2\lambda_2^2 - \bar{W}_3\lambda_3^2\right) - \bar{S}_2\lambda_2 \left(\bar{W}_3\lambda_3^2 - \bar{W}_1\lambda_1^2\right) + \bar{S}_3\lambda_3 \left(\bar{W}_1\lambda_1^2 - \bar{W}_2\lambda_2^2\right)\right] \\
D_{\mathrm{TI}} &= \left[\bar{S}_1 \left(\bar{W}_3\lambda_3^2 - \bar{W}_2\lambda_2^2\right) - \bar{S}_2 \left(\bar{W}_3\lambda_3^2 - \bar{W}_1\lambda_1^2\right) + \bar{S}_3 \left(\bar{W}_2\lambda_2^2 - \bar{W}_1\lambda_1^2\right)\right]
\end{aligned}$$

and $\bar{f}(p) = \int_0^\infty f(t)\mathrm{e}^{-pt}\mathrm{d}t$ is the Laplace transform of function $f(t)$. The use of expressions for $B_i (i = 1, 2, 3)$ given by Eq. 28 in Eqs. 25 and 26 leads to solutions of

stress, chemical potential, and dilatation functions due to thermal loads in the transformed domain.

4.2 Mass Concentration Loads

Upon applying the Laplace transform to the boundary condition, Eq. 18, and using the formal solution, Eq. 21, we again obtain a system of three equations in unknowns $B_i (i = 1, 2, 3)$, the solution of which provides

$$B_i = \frac{C_0 \bar{f}(p) D_i^*}{pD^*}, \quad i = 1, 2, 3 \tag{30}$$

$$\Delta^* = \begin{cases} pD_{\mathrm{CG}}^*, & \text{for CG} \\ D_{\mathrm{CI}}^*, & \text{for CI} \end{cases} \tag{31}$$

$$D_1^* = \lambda_1 \left(\bar{S}_2 - \bar{S}_3\right), \quad D_2^* = \lambda_2 \left(\bar{S}_3 - \bar{S}_1\right), \quad D_3^* = \lambda_1 \left(\bar{S}_1 - \bar{S}_2\right)$$
$$D_{\mathrm{CG}}^* = \bar{S}_1 \left(\bar{W}_2 \lambda_2 - \bar{W}_3 \lambda_3\right) + \bar{S}_2 \left(\bar{W}_3 \lambda_3 - \bar{W}_1 \lambda_1\right) + \bar{S}_3 \left(\bar{W}_1 \lambda_1 - \bar{W}_3 \lambda_3\right)$$
$$D_{\mathrm{CI}}^* = \left[\bar{S}_1 \left(\bar{W}_3 \lambda_3^2 - \bar{W}_2 \lambda_2^2\right) - \bar{S}_2 \left(\bar{W}_3 \lambda_3^2 - \bar{W}_1 \lambda_1^2\right) + \bar{S}_3 \left(\bar{W}_2 \lambda_2^2 - \bar{W}_1 \lambda_1^2\right)\right]$$

Through the use of Eq. 30 in Eqs. 25 and 26, we obtain the stress, chemical potential, and dilatation functions due to a mass concentration load in the transformed domain.

$$\text{We take } f(t) = \begin{cases} \delta(t), & \text{for implusive load} \\ H(t), & \text{for continuous load} \\ \cos \omega t, & \text{for periodic load} \end{cases} \tag{32}$$

Upon applying the Laplace transform to Eq. 32, we obtain

$$\bar{f}(p) = \begin{cases} 1, & \text{for impulsive load} \\ \frac{1}{p}, & \text{for continuous load} \\ \frac{p}{p^2+\omega^2}, & \text{for periodic load} \end{cases} \tag{33}$$

Thus, the dilatation, stress, and chemical potential in the transformed domain can be obtained from Eqs. 25 and 26 with the help of Eq. 28. We obtain

$$\begin{bmatrix} \bar{e}(x, p) \\ \bar{\sigma}_{xx}(x, p) \\ \bar{P}(x, p) \end{bmatrix} = -p\theta_0 \bar{f}(p) \sum_{i=1}^{3} \begin{bmatrix} \lambda_i \\ 1/\lambda_i \\ -\bar{\omega}_b \tau_1 \bar{W}_i / \lambda_i \end{bmatrix} \frac{D_i}{D} \mathrm{e}^{-\lambda_i p x} \tag{34}$$

where D, $D_i (= 1, 2, 3)$ are given by Eq. 29 and $\bar{f}(p)$ is defined in Eq. 33.

The corresponding expressions for these functions for the case of mass concentration loads can be written from Eq. 31 by substituting C_0, D^*, and $D_i^* (i = 1, 2, 3)$ in place of θ_0, D, and $D_i (i = 1, 2, 3)$, respectively.

4.3 Thermoelastic Half-Space

In the absence of mass diffusion ($a = 0 = \beta_2 \Rightarrow \varepsilon_C = 0 = \bar{b}$), we have

$$\bar{W}_i = \begin{cases} 1, & i = 3 \\ 0, & i = 1, 2 \end{cases}, \quad \bar{S}_i = \begin{cases} S_i^*, & i = 1, 2 \\ 0, & i = 3 \end{cases} \tag{35}$$

so that Eq. 24 lead to

$$\lambda_1^{*2} + \lambda_2^{*2} = 1 + \tau_0(1 + \varepsilon_T), \quad \lambda_1^{*2}\lambda_2^{*2} = \tau_0, \quad \lambda_3^{*2} = \bar{\omega}_b \tau_1 \tag{36}$$

In this case, the dilatation and temperature fields in the transformed domain due to the action of a TG are given by

$$\bar{e}(x, p) = -\frac{\theta_0 \bar{f}(p)}{p\left(\bar{S}_2^* \lambda_2^{*2} - \bar{S}_1^* \lambda_1^{*2}\right)} \left(\lambda_1^{*2} \exp\left(-\lambda_1^* px\right) - \lambda_2^{*2} \exp\left(-\lambda_2^* px\right)\right) \tag{37}$$

$$\sigma_{xx}(x, p) = -\frac{\theta_0 \bar{f}(p) \lambda_3^{*2}}{p\left(\bar{S}_2^* \lambda_2^{*2} - \bar{S}_1^* \lambda_1^{*2}\right)} \left(\exp\left(-\lambda_1^* px\right) - \exp\left(-\lambda_2^* px\right)\right) \tag{38}$$

where $\bar{S}_i^* = 1 - \lambda_i^{*2}$. In the case of TI, the above transformed functions become

$$\bar{e}(x, p) = -\frac{\theta_0 \bar{f}(p)}{\left(\bar{S}_2^* - \bar{S}_1^*\right)} \left\{\lambda_1^{*2} \exp\left(-\lambda_1^* px\right) - \lambda_2^{*2} \exp\left(-\lambda_2^* px\right)\right\} \tag{39}$$

$$\sigma_{xx}(x, p) = -\frac{\theta_0 \bar{f}(p) \lambda_3^{*2}}{\left(\bar{S}_2^* - \bar{S}_1^*\right)} \left\{\exp\left(-\lambda_1^* px\right) - \exp\left(-\lambda_2^* px\right)\right\} \tag{40}$$

5 Small-Time Approximations

Because of the damping term in Eq. 9, the dependence of roots λ_i on p is complicated and, hence, the inversion of the Laplace transform is quite difficult because the isolation of p is not possible. These difficulties, however, are reduced if we use some approximation or numerical methods. Because the 'second sound' effects are of short duration, we take p large. The roots $\lambda_i (i = 1, 2, 3)$ of Eq. 23 may be expanded binomially and after retaining only the positive sign, we obtain

$$\lambda_i = \frac{1}{V_i} + \frac{\phi_i}{p} + O\left(\frac{1}{p^2}\right), \quad i = 1, 2, 3 \tag{41}$$

$$\sum \frac{1}{V_1^2} = \frac{1 + \bar{\omega}_b t_1 + t_0\left\{\left(1 + \bar{a}\bar{b}\right)(1 + \varepsilon_a) + \left(1 + \bar{\beta}\bar{b}\right)(\varepsilon_T - \varepsilon_a)\right\}}{1 - \bar{\beta}\varepsilon_C}$$

$$\sum \frac{1}{V_1^2 V_2^2} = \frac{t_0(1 + \bar{a}\bar{b}) + \bar{\omega}_b t_1\{1 + t_0(1 + \varepsilon_T)\}}{1 - \bar{\beta}\varepsilon_C}$$

$$\sum \frac{1}{V_1^2 V_2^2 V_3^2} = \frac{\bar{\omega}_b t_1 t_0}{1 - \bar{\beta}\varepsilon_C} \tag{42}$$

$$\phi_i = \frac{A^* V_i^4 - B^* V_i^2 + C^*}{V_i\{(V_j^2 - V_i^2)(V_k^2 - V_i^2)}, \quad i \neq j \neq k = 1, 2, 3 \tag{43}$$

$$A^* = \frac{t_1 + t_0}{2t_1 t_0}$$

$$B^* = \frac{(1 + \bar{a}\bar{b}) + \bar{\omega}_b\{1 + (t_1 + t_0)(1 + \varepsilon_T)}{2\bar{\omega}_b t_1 t_0} \tag{44}$$

$$C^* = \frac{\bar{\omega}_b t_0 (1 + \bar{a}\bar{b})(1 + \varepsilon_a)}{2\bar{\omega}_b t_1 t_0}$$

The deformation, stress, and chemical potential in the case of a TG acting on the surface of the half-space are obtained as

$$\bar{e}(x, p) = -\theta_0 \sum_{i=1}^{3} \frac{D_{i0}\bar{f}(p)}{pD_0 V_i} e^{-\frac{x}{V_i}p} e^{-\phi_i x} \tag{45}$$

$$\bar{\sigma}_{xx}(x, p) = -\theta_0 \sum_{i=1}^{3} \frac{D_{i0} V_i \bar{f}(p)}{pD_0} e^{-\frac{x}{V_i}p} e^{-\phi_i x} \tag{46}$$

$$\bar{P}(x, p) = \theta_0 \sum_{i=1}^{3} \frac{\bar{\omega}_b W_{i0} t_1 D_{i0} \bar{f}(p) V_i}{pD_0} e^{-\frac{x}{V_i}} e^{-\phi_i x} \tag{47}$$

where

$$D_{10} = \frac{1}{V_1}\left(\frac{\bar{W}_{20}}{V_2^2} - \frac{\bar{W}_{30}}{V_3^2}\right), D_{20} = \frac{1}{V_2}\left(\frac{\bar{W}_{30}}{V_2^2} - \frac{\bar{W}_{10}}{V_1^2}\right), \tag{48}$$

$$D_{30} = \frac{1}{V_3}\left(\frac{\bar{W}_{10}}{V_1^2} - \frac{\bar{W}_{20}}{V_2^2}\right)$$

$$D_0 = \sum_{(i,j,k)} \frac{W_{k0}}{V_k^2}\left\{\frac{1}{V_i^2} - \frac{1}{V_j^2} + \bar{\beta}\left(\frac{\bar{W}_{i0}}{V_i^2} - \frac{\bar{W}_{j0}}{V_j^2}\right)\right\}$$

$$\bar{W}_{i0} = \frac{\left(V_i^2 - 1 - \varepsilon_a\right)\bar{b}}{1 + \bar{\beta}\bar{b} - \bar{\omega}_b t_1 V_i^2} \tag{49}$$

Here, $(i, j, k) = (1, 2, 3)$, $(2, 3, 1)$, and $(3, 1, 2)$. Inverting the Laplace transform of Eqs. 45–47, the solution of the considered functions in the physical domain is obtained as

$$e(x, t) = -\theta_0 \sum_{i=1}^{3} \frac{D_{i0}}{D_0 V_i} \exp\{-\phi_i x\} F_i(x, t) \tag{50.1}$$

$$\sigma_{xx}(x,t) = -\theta_0 \sum_{i=1}^{3} \frac{D_{i0} V_i}{D_0} \exp\{-\phi_i x\} F_i(x,t) \tag{50.2}$$

$$P(x,t) = \theta_0 \sum_{i=1}^{3} \frac{D_{i0} \bar{W}_{i0} \bar{\omega}_b t_1 V_i}{D_0} \exp\{-\phi_i x\} F_i(x,t) \tag{50.3}$$

where

$$F_i(x,t) = \begin{cases} H(t - \frac{x}{V_i}), & \text{for impulsive load} \\ \left(t - \frac{x}{V_i}\right) H\left(t - \frac{x}{V_i}\right), & \text{for continuous load} \\ \frac{\sin \omega\left(t - \frac{x}{V_i}\right)}{\omega}, & \text{for periodic load} \end{cases}$$

Here, $H(t - \frac{x}{V_i})$ represents Heaviside unit step functions. In the case of TI, the above functions are obtained as

$$\bar{e}\,(x,t) = -\theta_0 \sum_{i=1}^{3} \frac{D_{i0}}{D_0 V_i} \exp\{-\phi_i x\} G_i\,(x,t) \tag{50.4}$$

$$\sigma_{xx}\,(x,t) = -\theta_0 \sum_{i=1}^{3} \frac{D_{i0} V_i}{D_0} \exp\{-\phi_i x\} G_i\,(x,t) \tag{50.5}$$

$$P\,(x,t) = -\theta_0 \sum_{i=1}^{3} \frac{D_{i0} \bar{\omega}_b \bar{W}_{io} t_1 V_i}{D_0} \exp\{-\phi_i x\} G_i\,(x,t) \tag{50.6}$$

where

$$G_i(x,t) = \begin{cases} \delta\left(t - \frac{x}{V_i}\right) & \text{for impact load} \\ H\left(t - \frac{x}{V_i}\right), & \text{for continuous load} \\ \cos \omega\left(t - \frac{x}{V_i}\right) & \text{for periodic load} \end{cases}$$

Similar expressions can be obtained for the mass concentration load by employing the above approach.

5.1 Approximation for Thermoelastic Half-Space

For large p, Eq. 36 with the help of expression,

$$\lambda_i^* = \frac{1}{V_i^*} + \frac{\phi_i^*}{p} + O\left(\frac{1}{p^2}\right), \quad i = 1, 2$$

provide us with

$$V_1^{*-2} + V_2^{*-2} = 1 + t_0(1+\varepsilon_T), \quad V_1^{*-2} V_2^{*-2} = t_0, \quad V_3^{*-2} = \bar{\omega}_b t_1 \tag{51}$$

$$\phi_i^* = \frac{V_1^* V_2^* N_1}{2\left(V_1^{*2} - V_2^{*2}\right)}, \quad \phi_2^* = \frac{V_1^* V_2^* N_2}{V_1^{*2} - V_2^{*2}} \tag{52}$$

$$N_1 = V_1^*\left(V_1^* + V_2^*\right) - V_2^*\left(1+\varepsilon_{\mathrm{T}}\right),$$

$$N_2 = V_2^*\left(V_1^* + V_2^*\right) - V_1^*\left(1+\varepsilon_{\mathrm{T}}\right) \tag{53}$$

Equation 51 implies that

$$\frac{1}{V_1^{*2}}, \frac{1}{V_2^{*2}} = \frac{1 + t_0(1+\varepsilon_{\mathrm{T}}) \pm \sqrt{M}}{2} \tag{54}$$

where $M = \sqrt{\{1 - t_0(1+\varepsilon_T)\}^2 + 4\varepsilon_T t_0} = \frac{1}{V_1^{*2}} - \frac{1}{V_2^{*2}} > 0$.

This clearly shows that $M > 0$ and, hence, $V_1^* < V_2^*$. Thus, V_1^* corresponds to the slowest wave and V_2^* refers to the fastest wave. Furthermore, in the absence of thermo-mechanical coupling ($\varepsilon_{\mathrm{T}} = 0$), Eq. 54 leads to

$$V_2^* = \frac{1}{\sqrt{t_0}}, \quad V_1^* = 1, \quad V_3^* = \frac{1}{\sqrt{\varpi_b t_1}} \tag{55}$$

Here, V_1^* corresponds to an elasto-diffusive wave and V_2^* refers to a thermo-diffusive wave. For most of the materials, t_0 is quite small, and therefore $V_1^* < V_2^*$ and, thus, the elasto-diffusive wave follows the thermo-diffusive wave. Moreover, the thermo-diffusive waves have a finite, although quite large, velocity of propagation. In the absence of relaxation times ($t_1 = t_0 = 0$), Eq. 55 provides us with

$$V_2^* \to \infty, \quad V_3^* \to \infty, \quad V_1^* = 1$$

This implies that in the absence of thermal relaxation times, the elasto-diffusive wave becomes the longitudinal elastic wave and travels with a velocity $c_{\mathrm{L}}^2 = \frac{(\lambda+2\mu)}{\rho}$ as in elasto-kinetics, and the other two waves have an infinite velocity of propagation being diffusive in character. This corresponds to the case of conventional coupled thermo-elasticity which predict an infinite speed of heat propagation and mass diffusion.

The dilatation and stress in the transformed domain given by Eqs. 39 and 40 in the case of a small time approximation become

$$\bar{e}(x,\, p) = -\frac{\theta_0 \bar{f}(p)}{pV'}\left(V_1^* V_2^{*3} \mathrm{e}^{-\frac{x}{V_1^*}p} \mathrm{e}^{-\phi_1^* x} + V_1^{*3} V_2^* \mathrm{e}^{-\frac{x}{V_2^*}p} \mathrm{e}^{-\phi_2^* x}\right) \tag{56}$$

$$\sigma_{xx}\,(x,\, p) = -\frac{\theta_0 \bar{f}\,(p)\, V_1^{*3} V_2^{*3}}{pV'}\left(\mathrm{e}^{-\frac{x}{V_1^*}p} \mathrm{e}^{-\phi_1^* x} + \mathrm{e}^{-\frac{x}{V_2^*}p} \mathrm{e}^{-\phi_2^* x}\right) \tag{57}$$

Inverting the Laplace transform in the above expressions, for the case of a TG, we get

$$\begin{aligned} e(x,t) &= -\frac{\theta_0}{V'}\sum_{\substack{i=1\\ j\neq i}}^{2} V_i^* V_j^{*2}\exp\{-\phi_i^* x\}F_i^*(x,t) \\ \sigma_{xx}(x,t) &= -\frac{\theta_0 V_1^{*3} V_2^{*3}}{V'}\sum_{i=1}^{2}\exp\{-\phi_i^* x\}F_i^*(x,t) \end{aligned} \tag{58.1}$$

where $V' = \left(V_2^* - V_1^*\right)\left\{V_1^{*2} + V_2^{*2} + V_1^{*2}V_2^{*2} + 1\right\}$

$$F_i^*(x,t) = \begin{cases} H\left(t - \frac{x}{V_i^*}\right), & \text{for impulsive load} \\ \left(t - \frac{x}{V_i^*}\right)H\left(t - \frac{x}{V_i^*}\right), & \text{for continuous load} \\ \frac{\sin\omega\left(t - \frac{x}{V_i^*}\right)}{\omega}, & \text{for periodic load} \end{cases}$$

Similarly, in the case of TI, the above expressions become

$$\begin{aligned} e(x,t) &= -\frac{\theta_0}{V_1^{*2} - V_2^{*2}}\sum_{i=1}^{2} V_i^{*2}\exp(\phi_i x)G_i^*(x,t) \\ \sigma_{xx}(x,t) &= -\frac{\theta_0}{V_1^{*2} - V_2^{*2}}\sum_{i=1}^{2}\exp(\phi_i x)G_i^*(x,t) \end{aligned} \tag{58.2}$$

where

$$G_i^*(x,t) = \begin{cases} \delta\left(t - \frac{x}{V_i^*}\right), & \text{for impulsive load} \\ H\left(t - \frac{x}{V_i^*}\right), & \text{for continuous load} \\ \cos\omega\left(t - \frac{x}{V_i^*}\right), & \text{for periodic load} \end{cases}$$

Clearly, these solutions are contributed by elastic and thermal waves.

6 Discussion of Results at Wave Fronts

The short-time solutions obtained above indicate that each of the functions e, P, and σ_{xx} is made up of three waves, namely, elasto-diffusive, thermo-diffusive, and mass-diffusive traveling waves with finite velocities V_1, V_2, and V_3, respectively. The presence of Heaviside functions $H(t - \frac{x}{V_i})$ indicates that $x = V_i t,\ i = 1, 2, 3$ are the probable discontinuous points of e, P, and σ_{xx}. The jumps at the wave fronts due to

a TG acting at the surface of half-space are given by

$$\left[e^{+}-e^{-}\right]_{V_i t}=-\theta_0\begin{cases}\frac{D_{i0}}{D_0 V_i}\exp\left(-\phi_i V_i t\right), & \text{for impulsive load}\\ 0, & \text{for continuous and periodic loads}\end{cases} \tag{59.1}$$

$$\left[\sigma_{xx}^{+}-\sigma_{xx}^{-}\right]_{V_i t}=-\theta_0\begin{cases}\frac{D_{i0}}{D_0 V_i}\exp\left(-\phi_i V_i t\right), & \text{for impulsive load}\\ 0, & \text{for continuous and periodic loads}\end{cases} \tag{59.2}$$

$$\left[P^{+}-P^{-}\right]_{V_i t}=\theta_0\begin{cases}\frac{D_{i0}\bar{W}_{i0}\bar{\omega}_b t_1}{D_0}\exp\left(-\phi_i V_i t\right), & \text{for impulsive load}\\ 0, & \text{for continuous and periodic loads}\end{cases} \tag{59.3}$$

In case of a TI, the jumps in various considered functions are obtained as

$$\left[e^{+}-e^{-}\right]_{V_i t}=-\theta_0\begin{cases}\infty, & \text{for impulsive load}\\ \frac{D_{i0}}{D_0 V_i}\exp\left(-\phi_i V_i t\right), & \text{for continuous and periodic loads}\end{cases} \tag{60.1}$$

$$\left[\sigma_{xx}^{+}-\sigma_{xx}^{-}\right]_{V_i t}=-\theta_0\begin{cases}\infty, & \text{for impulsive load}\\ \frac{D_{i0}}{D_0 V_i}\exp\left(-\phi_i V_i t\right), & \text{for continuous and periodic loads}\end{cases} \tag{60.2}$$

$$\left[P^{+}-P^{-}\right]_{V_i t}=\theta_0\begin{cases}\infty, & \text{for impulsive load}\\ \frac{D_{i0}}{D_0 V_i}\exp\left(-\phi_i V_i t\right), & \text{for continuous and periodic loads}\end{cases} \tag{60.3}$$

The disturbance in the medium consists of three coupled waves, one following the other. For most of the materials, the faster wave is the elastic wave and the thermal wave is slower than the elastic wave but faster than the mass diffusive wave. The above expressions show that the dilatation, stress, and chemical potential are continuous at each wave front for continuous and periodic loads in the case of a TG input acting at the boundary of the half-space. However, these functions are discontinuous at wave fronts in the case of an impulsive load. This means that a discontinuous load does generate discontinuities in the dilatation which is not physically realistic.

The jumps at the wave fronts due to a TG and a TI applied on the surface of a thermoelastic (in the absence of mass diffusion) half-space are, respectively, given

by

$$\left(e^{+}-e^{-}\right)_{x=V_i^* t}=\begin{cases}0, & \text{for continuous and periodic loads}\\ \frac{\theta_0 V_i^{*2}}{\left(\bar{S}_1^*\lambda_1^{*2}-\bar{S}_2^*\lambda_2^{*2}\right)}\mathrm{e}^{-\phi_i^* V_i^* t}, & \text{for impulsive load}\end{cases}$$

$$\left(\sigma_{xx}^{+}-\sigma_{xx}^{-}\right)_{x=V_i^* t}=\begin{cases}0, & \text{for impulsive and periodic loads}\\ \frac{\theta_0}{\left(\bar{S}_2^*\lambda_2^{*2}-\bar{S}_1^*\lambda_1^{*2}\right)}\mathrm{e}^{-\phi_i^* V_i^* t}, & \text{for continuous load}\end{cases} \tag{61.1}$$

$$\left(e^{+}-e^{-}\right)_{x=V_i^* t}=\begin{cases}0, & \text{for impulsive load}\\ \frac{\theta_0 V_i^{*2}}{V_2^{*2}-V_1^{*2}}\mathrm{e}^{-\phi_i^* V_i^* t}, & \text{for continuous and periodic loads}\end{cases}$$

$$\left(\sigma_{xx}^{+}-\sigma_{xx}^{-}\right)_{x=V_i^* t}=\begin{cases}0, & \text{for continuous load}\\ \frac{\theta_0}{V_2^{*2}-V_1^{*2}}\mathrm{e}^{-\phi_i^* V_i^* t}, & \text{for impulsive and periodic loads}\end{cases} \tag{61.2}$$

Clearly, the jumps at the wave fronts in these functions are exponentially decaying with time.

7 Laplace Transform Inversion and Physical Solution

In this section, we will find a solution in the physical domain at all times by employing a numerical technique of the Laplace transform inversion. To obtain the solution of the problem in the physical domain, we must invert the Laplace transform in Eqs. 34 and 37–40. The Laplace transform of each function in these equations is given by

$$\bar{g}(x,p)=\int_0^\infty g(x,t)\mathrm{e}^{-pt}\mathrm{d}t \tag{62}$$

The inversion formula for the Laplace transform is

$$g(t)=\frac{1}{2\pi i}\int_{\gamma-i\infty}^{\gamma+i\infty}\bar{g}(p)\,\mathrm{e}^{pt}\mathrm{d}p \tag{63}$$

where γ is an arbitrary real number greater than all real parts of all the singularities of $\bar{g}(p)$. The above integral can be solved by setting $p=\gamma+iy$; we get

$$g(t)=\frac{\mathrm{e}^{\gamma t}}{2\pi}\int_{-\infty}^{+\infty}\bar{g}(\gamma+iy)\mathrm{e}^{ity}\mathrm{d}y \tag{64}$$

Let $h(t)=g(t)\mathrm{e}^{-\gamma t}$ while expanding the function $g(t)\mathrm{e}^{-\gamma t}$ in a Fourier series in the interval $[0,2l]$, we obtain the approximation formula as

$$g(t)=g_\infty(t)+E_\mathrm{D}$$

where

$$g_\infty(t) = \frac{C_0}{2} + \sum_{k=1}^{\infty} C_K, \quad \text{for } 0 \le t \le 2l \tag{65}$$

Here,

$$C_k = \frac{\exp(\gamma t)}{l} \Re\mathfrak{e}\left[\bar{g}\left(\gamma + \frac{ik\pi}{l}\right)\exp\left(\frac{ik\pi t}{l}\right)\right]$$

and E_{D} is the discretization error that can be made arbitrarily small by choosing γ sufficiently large.

As the infinite series in Eq. 63 can be summed to a finite number N of terms, the approximate value of $g(t)$ becomes

$$g_N(t) = \frac{C_0}{2} + \sum_{k=1}^{N} C_K, \quad \text{for all } 0 \le t \le 2l \tag{66}$$

Using this formula to evaluate $g(t)$, a new error called the truncation error is introduced that must be added to the discretization error to produce the total approximation error. The Korrector method is used to reduce the discretization error; while the ε-algorithmic method is used to reduce the truncation error and, hence, to accelerate the convergence. The Korrector method is used to evaluate the function $g(t)$,

$$g(t) = g_\infty(t) - \exp(-2\gamma l) g_\infty(2l + t) + E'_D$$

where $\left|E'_D\right| < |E_{D.}|$, the approximate value of $g(t)$ becomes

$$g_{N_K}(t) = g_N(t) - \exp(-2\gamma l)\, g'_{\dot{N}}(2l + 1) \tag{67}$$

where N is an integer such that $N' < N$.

We shall now describe the ε-algorithm method used to accelerate the convergence of the series. Let N be an odd natural number and let $s_m = \sum_{K=1}^{N} C_K$ be the sum of partial sequences of Eq. 65. We define the ε sequence by

$$\varepsilon_{0,m} = 0, \quad \varepsilon_{1,m} = s_m, \quad \varepsilon_{n+1,m} = \varepsilon_{n-1,m+1} - \frac{1}{\varepsilon_{n,m+1} - \varepsilon_{n,m}}, \quad n, m = 1, 2, 3$$

It can be shown that the sequence of partial sums $\varepsilon_{1,1}, \varepsilon_{3,1}, \ldots, \varepsilon_{N+1}$ converges to $g(t) + E_D - \frac{C_0}{2}$ faster than the sequence of partial sums $(s_m,\ m = 1, 2, 3, \ldots)$.

The actual procedure used to invert the Laplace transform consists of Eq. 66 together with the ε-algorithm. The values of γ and l are chosen according to the criteria outlined in Honig and Hirdes [20].

Table 1 Physical data for brass (70 % Cu + 30 % Zn) and Cu materials

Coefficient	Unit	Brass	Copper	References
λ	$N \cdot m^{-2}$	7.69×10^{10}	7.76×10^{10}	Callister, Jr. [22]
μ	$N \cdot m^{-2}$	3.61×10^{10}	3.86×10^{10}	Callister, Jr. [22]
ρ	$kg \cdot m^{-3}$	8.522×10^{3}	8.954×10^{3}	Thomas [23]
C_e	$J \cdot kg^{-1} \cdot K^{-1}$	385	383.1	Thomas [23]
K	$W \cdot m^{-1} \cdot K^{-1}$	1.11×10^{2}	386	Thomas [23]
α_T	K^{-1}	2×10^{-6}	1.78×10^{-5}	Thomas [23]
D	$m^2 \cdot s^{-1}$	0.24×10^{-4}	0.85×10^{-8}	Callister, Jr. [22]
α_C	K^{-1}	1.8×10^{-5}	1.98×10^{-4}	Callister, Jr. [22]
a	$m \cdot S^{-1}$	0.1521×10^{2}	1.2×10^{4}	Sherief and Saleh [15]
b	$m \cdot S^{-1}$	0.02×10^{4}	9×10^{6}	Sherief and Saleh [15]
T_0	K	293	293	Thomas [23]

8 Numerical Results and Discussion

To illustrate the analytical results obtained in the pervious section, we present some numerical simulation results. The materials chosen for the purpose of numerical calculations are brass (70 % Cu + 30 % Zn) and copper (Cu) whose physical data are given in Table 1. The dimensional values of thermal relaxation time parameters t_0 have been estimated from Eq. 2.5 of Chandrasekharaiah [21] and that of t_1 is taken as proportional to t_0. Consequently, the dimensionless values of thermal relaxation times have been taken as $t_0 = 0.5$ and $t_1 = 0.3$ for computation purposes. The dimensionless dilatation, chemical potential, and stress functions have been computed for brass and Cu materials for two values of time ($t = 0.5, 0.75$) at different locations (x) from Eq. 34. However, the equivalent results in dimensional form with respect to these considered field functions can be obtained by using quantities in Eq. 11. The computer-simulated results have been plotted graphically for the cases of TI and concentration input (CI) applications on the boundary of the half-space in Figs. 1 –15. The profiles with a ball represent Cu and those without a ball refer to brass materials.

8.1 Temperature Input

Figure 1 shows the variation of the dilatation (e) with distance (x) due to instantaneous application of the TI acting on the surface of the half-space. It is observed that at time $t = 0.50$, the magnitude of dilatation for the case of brass increases for $0 \leq x \leq 0.5$ in the vicinity of the load and a sharp decrease is observed for $0.5 \leq x \leq 1$, before it starts behaving in a sinusoidal manner in the range $1 \leq x \leq 2.5$. The profile of this quantity is observed to become asymptotically close to zero at $x \geq 4$. At time $t = 0.75$, the magnitude of variations of this quantity increases monotonically for $0 \leq x \leq 0.50$, decreases for $0.5 \leq x \leq 1$, and then follows a sinusoidal pattern in the range $1 \leq x \leq 2.5$ before asymptotically tending to zero for $x \geq 4$ after observing a steady increase for the case of the brass material. It is observed that the corresponding

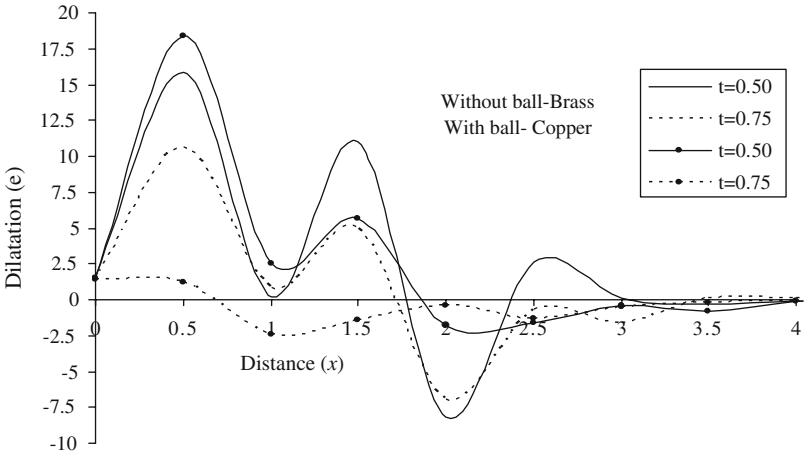

Fig. 1 Variation of dilatation due to instantaneous TI

profiles of dilatation for the copper material at both values of time ($t = 0.50$ and $t = 0.75$) almost follow closely those of brass and hence exhibit a similar behavior.

Figure 2 presents the variations of the chemical potential distribution with distance due to instantaneous application of a TI acting on the surface of the copper and brass half-spaces at $t = 0.50$ and $t = 0.75$. The chemical potential distribution for the case of the brass material at $t = 0.50$ is found to increase sharply in the domain $0 \leq x \leq 0.50$, decreases for $0.50 \leq x \leq 1$, and oscillates in the range $1 \leq x \leq 4$ before it starts decreasing to become asymptotically close to zero at $x \geq 4$. At time $t = 0.75$, the trend of variations of the profile of this quantity is found to be similar to that at $t = 0.50$ except there are some changes in its magnitude for the case of the brass material. The trend of variations of the chemical potential in Cu also follows an almost similar pattern to that of the brass material with the exception that its magnitude is less than that in the case of the brass material.

Figure 3 shows variations of the stress distribution with distance (x) due to instantaneous application of a TI on the half-space. It is found that at $t = 0.50$, the magnitude of stress increases sharply in the range $0 \leq x \leq 0.50$, decreases monotonically for $0.50 \leq x \leq 3.5$, and becomes steady before ultimately tending to zero at $x \geq 4$. At $t = 0.75$, the stress magnitude increases in the range $0 \leq x \leq 1.5$, becomes almost uniform in the domain $1.5 \leq x \leq 2$, and decreases for $3 \leq x \leq 3.5$, before it becomes steady and asymptotically close to zero at $x \geq 4$. The trend of variations of the stress magnitude in the Cu material at $t = 0.50$ is found to follow an almost similar pattern as observed in the case of brass at the time with the exception of its distinguished trend in the range of $1.5 \leq x \leq 3$. It is also observed from the graph that at time $t = 0.75$, the profile for the copper material shows an increasing trend in the region $0 \leq x \leq 0.50$, remains uniform for $0.50 \leq x \leq 3$, and decreases monotonically in the domain $x \geq 3.5$ before it becomes steady and stable for $x \geq 4$. It is noticed that the stress remains tensile for both brass and Cu materials due to instantaneous application of TI at both considered values of time.

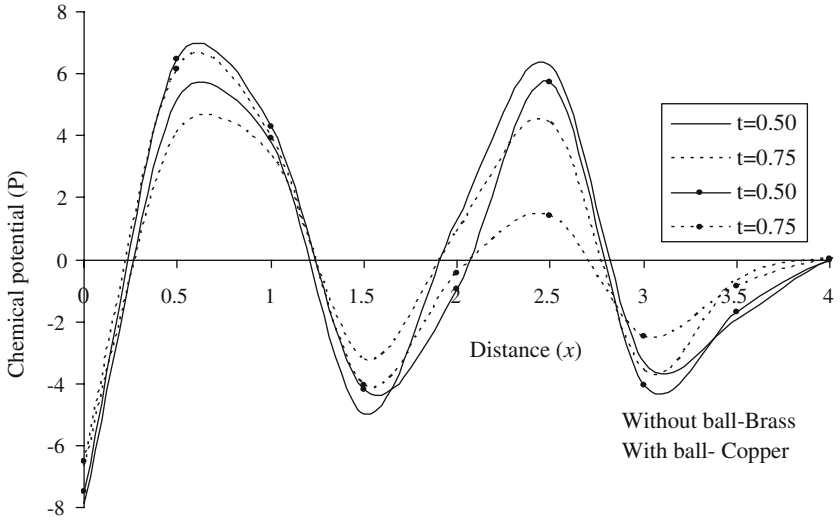

Fig. 2 Variation of chemical potential due to instantaneous TI

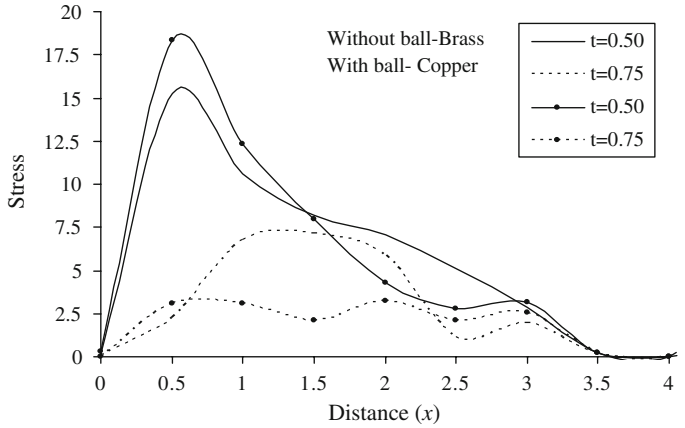

Fig. 3 Distribution of stress due to instantaneous TI

Figure 4 presents the variations of the dilatation due to continuous application of a TI on the boundary of the half-space. It is observed that at $t = 0.50$, the magnitude of the dilatation in brass decreases sharply in the domain $0 \leq x \leq 0.50$, remains uniform for $0.50 \leq x \leq 2$, and increases monotonically in the range $2 \leq x \leq 4$ to become steady and asymptotically close to zero for $x \geq 8$. At time $t = 0.75$, the profile of this quantity follows a decreasing trend in the range $0 \leq x \leq 1$, which increases sharply for $1 \leq x \leq 2$, and shows a dipping behavior at $x \geq 3$, before it asymptotically tends to zero for $x \geq 8$ after observing a slight increase in the domain $3 \leq x \leq 4$. For the case of a Cu material, the profile of this quantity follows almost a similar trend of variation as that of the brass material at $t = 0.50$ and $t = 0.75$ with the exception of its distinct variation in the range $0.50 \leq x \leq 1.5$ at $t = 0.50$.

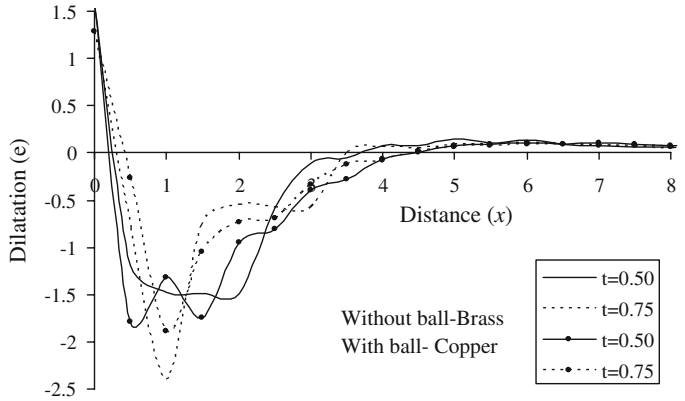

Fig. 4 Variation of dilatation due to continuous TI

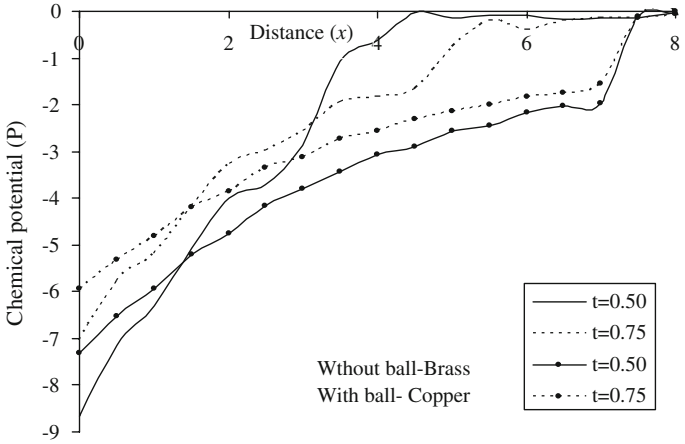

Fig. 5 Distributions chemical potential due to continuous TI

Figure 5 represents the distribution of the chemical potential due to a continuously applied TI on the boundary of the considered half-space. It is revealed that the trend of variations of this quantity at $t = 0.50$ for the brass material shows a sharp increase in the range $0 \leq x \leq 2$, with a slight dipping behavior in the domain $2 \leq x \leq 4$, before it increases to become asymptotically close to zero at $x \geq 8$. At $t = 0.75$, the trend of variations of the chemical potential remains almost the same, although having less magnitude as compared to that at $t = 0.50$. The variation of the profiles of the chemical potential for Cu material is found to increase monotonically in the range $0 \leq x \leq 6.5$ and shows a slightly decreasing trend for $6.5 \leq x \leq 7$ to become asymptotically close to zero at $x \geq 8$ at the considered values of time.

Figure 6 shows the distribution of the stress due to continuous application of a TI on the surface of the half-space with distance (x). For the brass material, the trend of variations of the stress magnitude at $t = 0.50$ is found to increase in the range $0.5 \leq x \leq 1.5$, exhibits dipping behavior in the domain $1.5 \leq x \leq 2$, and again starts

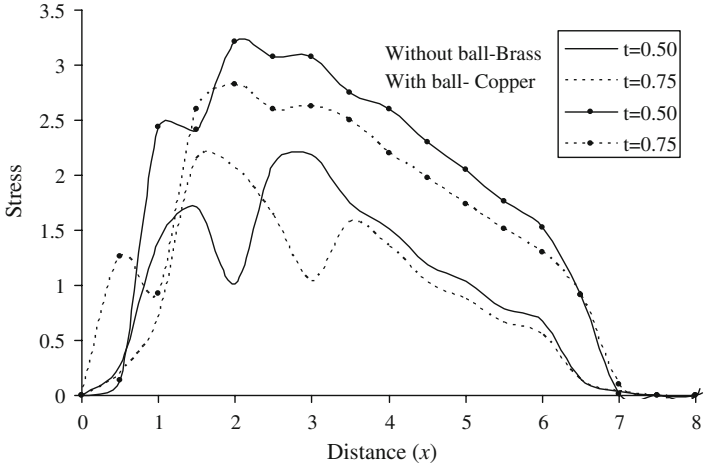

Fig. 6 Distribution of stress due to continuous TI

increasing for $2 \leq x \leq 3$, before it decreases monotonically to become asymptotically close to zero at $x \geq 8$. At $t = 0.75$, the profile of this quantity follows an increasing trend in the range $0 \leq x \leq 2$, which decreases for $2 \leq x \leq 3$ and again observes a slight increase in the domain $3 \leq x \leq 4$, before it decreases monotonically in the range $4 \leq x \leq 6$ to become approximately close to zero for $x \geq 7$. The profiles of variations of the stress magnitude for the Cu material at $t = 0.50$ and $t = 0.75$ increase sharply in the range $0 \leq x \leq 1.5$ with a slight dip in the region $1.5 \leq x \leq 3$ and then decrease monotonically in the domain $3 \leq x \leq 7$ to become asymptotically close to zero for $x \geq 7$. The stress is observed to be tensile in both materials at the considered values of time due to a continuous TI application at the surface.

A comparison of Figs. 1–6 shows that all the considered field quantities observe maximum magnitudes of variations in their distribution in the vicinity of the thermal load which ultimately dies out with increasing distance and time. This convergence of results shows the existence of wave fronts. The magnitudes of computed quantities are found to be quite high in the case of an instantaneous source as compared to that for a continuous one. However, the profiles for the latter case travel longer distances than those of the former one which is consistent with the nature and character of the load in addition to the physical facts.

8.2 Concentration Input

Figure 7 presents the variations of the dilatation due to instantaneous application of a CI at the surface of the solid. It is observed that due to this type of loading, the magnitude of variations of the dilatation in both brass and Cu materials is approximately half of that due to a TI given in Fig. 1 at the considered times. At time $t = 0.50$, the dilatation profiles of brass and Cu materials follow a sinusoidal pattern before becoming asymptotically close to zero at $x \geq 3$ with the exceptions of magnitude variations

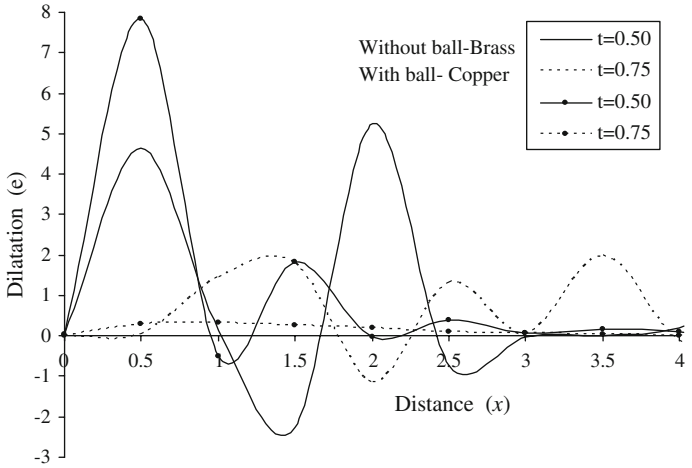

Fig. 7 Variation of dilatation due to instantaneous mass CI

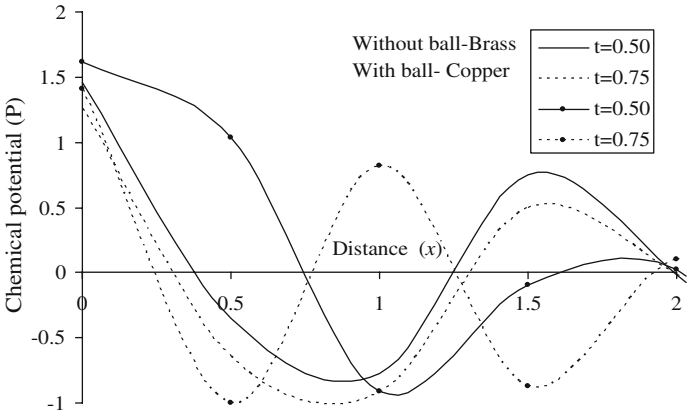

Fig. 8 Variation of chemical potential due to instantaneous mass CI

in certain ranges of the distance. The profiles of the dilatation in both materials at $t = 0.75$ also follow almost similar trends of variations except that the magnitude of this quantity falls drastically in comparison to that at $t = 0.50$ in addition to some phase shifts. The decreasing magnitude of this quantity with the passage of time is quite consistent with the physical facts.

Figure 8 represents the variations of the chemical potential due to instantaneous application of a CI at the surface of brass and Cu material half-spaces. Figure 8 reveals that the profiles of the chemical potential at $t = 0.50$ and $t = 0.75$ follow almost similar trends with increasing distance from the point of application of the load but with fluctuating behavior, becoming asymptotically close to zero for $x \geq 2$. However, the profiles corresponding to the Cu material at $t = 0.75$ are observed to be phase shifted after $x \geq 0.50$ in relation to that of the brass material at $t = 0.50$.

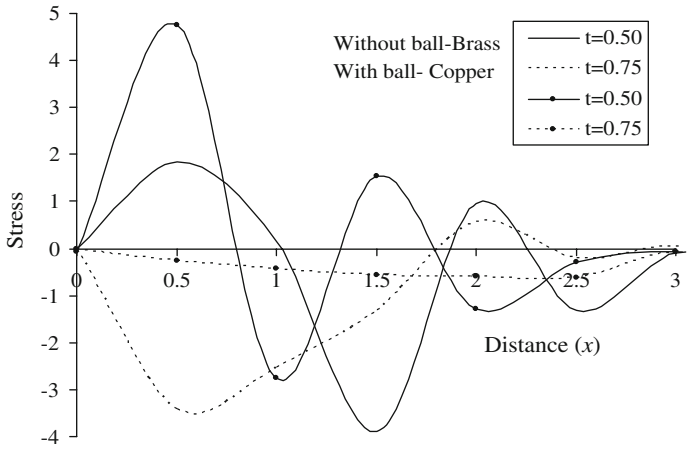

Fig. 9 Distribution of stress due to instantaneous mass CI

Figure 9 shows the variations of the stress due to instantaneous application of a CI. At $t = 0.50$, the stress distribution profile of the brass material increases in the domain $0 \leq x \leq 0.50$ and decreases sharply for $0.50 \leq x \leq 1.5$, before it starts increasing in the domain $1.5 \leq x \leq 2$ to become asymptotically close to zero for $x \geq 3$. At $t = 0.75$, the profiles of this quantity follow a decreasing trend in the range $0 \leq x \leq 1$, which increases in the domain $1 \leq x \leq 2$ and again decreases for $2 \leq x \leq 2.5$, before it starts increasing steadily to become asymptotically close to zero for $x \geq 3$. For a Cu material, the stress distribution profiles seem to follow a similar trend of variations with different magnitudes at $t = 0.50$ and $t = 0.75$.

Figures 10–12, respectively, show the variations of the dilatation, stress, and chemical potential due to continuous application of a CI on the surface of the half-space.

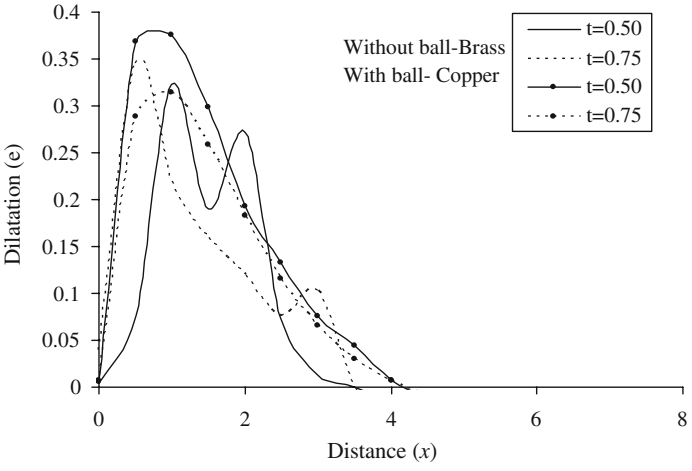

Fig. 10 Variation of dilatation due to continuous mass CI

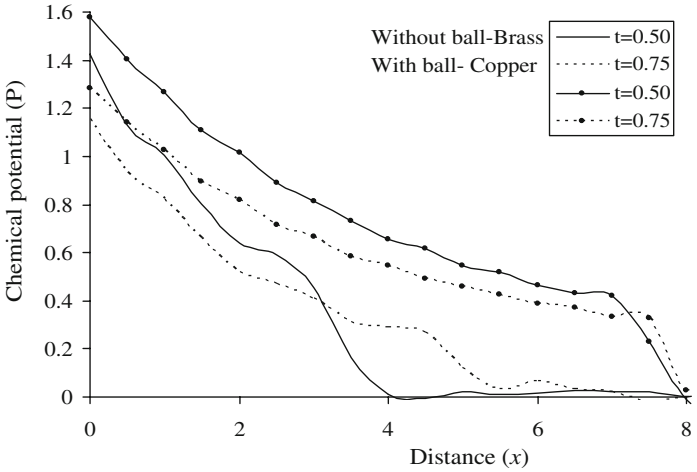

Fig. 11 Chemical potential distribution due to continuous mass CI

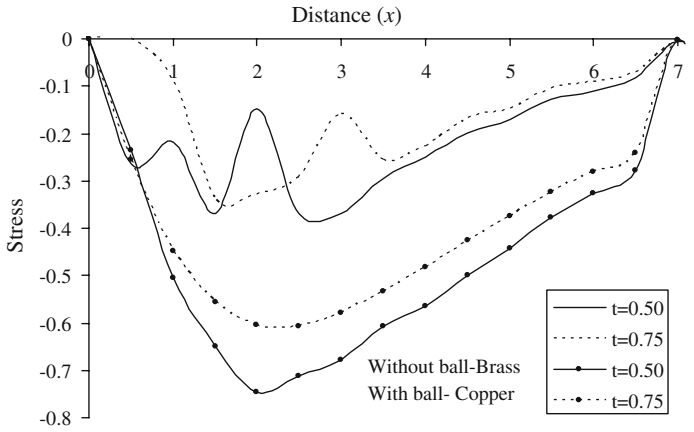

Fig. 12 Variation of stress due to continuous mass CI

It is observed that in brass and Cu materials, the distribution profiles of dilatation observed is quite opposite in trend in contrast to that of a continuous TI at $t = 0.50$ and $t = 0.75$. All these curves become asymptotically close to zero for $x \geq 8$ in both materials.

The comparison of Figs. 7–12 revealed that the application of a CI on the surface of the Cu or brass material resulted in similar types of effects as that produced by the TI in these materials. It is noticed that the stress which is tensile initially for the case of instantaneous loading becomes compressive with the passage of time. However, the stress remains compressive for the case of continuous loading under the considered conditions. The convergence of various profiles in these figures at certain distances again shows the existence of wave fronts and, hence, demonstrates the fact of a finite velocity, although large heat propagation in nonclassical thermoelasticity.

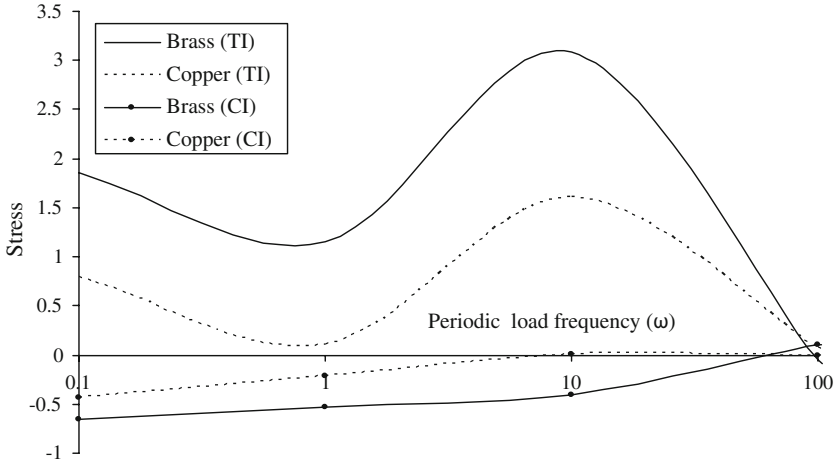

Fig. 13 Variation of dilatation with the frequency of periodic TI and CI loadings

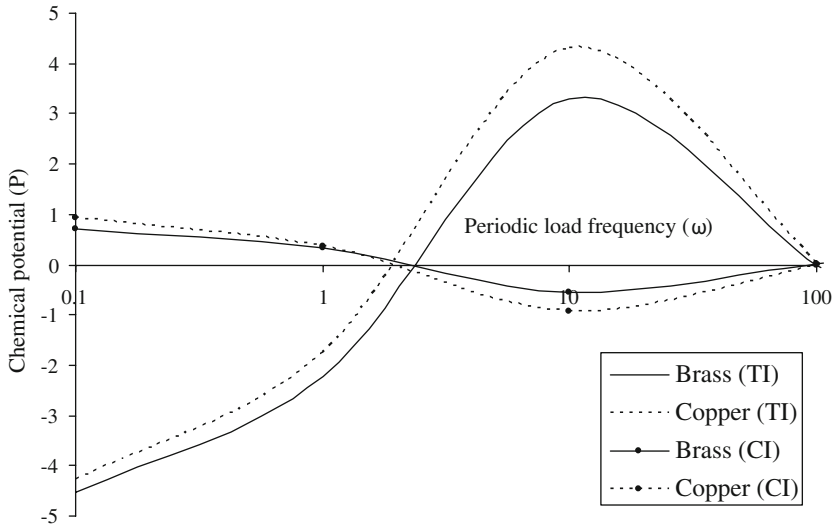

Fig. 14 Variation of chemical potential with the frequency of periodic TI and CI loadings

Figures 13–15 present variations of the dilatation, chemical potential, and stress due to the application of a periodic TI and a CI with the load frequency on log-linear scales. Here, solid curves correspond to brass, and dotted curves refer to Cu materials. The profiles with and without balls represent CI and TI, respectively. All the considered quantities are observed to vanish in a converging fashion after the periodic load frequency $\omega \geq 100$. The maximum variation (resonance condition) is observed to have occurred at $\omega = 10$ for the case of dilatation, stress, and chemical potential. To sum up, it is clear from the above discussion that all the considered functions vanish at certain finite values of distance, thereby showing the existence of wave fronts in the

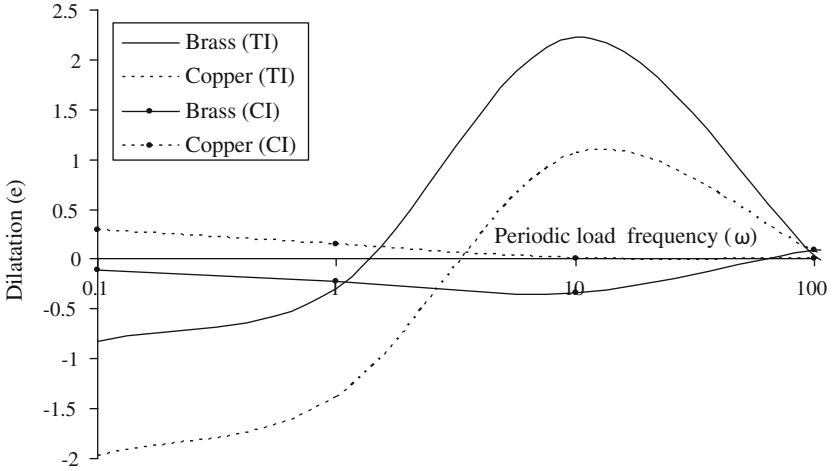

Fig. 15 Variation of stress with the frequency of periodic TI and CI loadings

case of nonclassical theory of thermoelasticity in contrast to that of classical theory where the solutions are predominantly diffusive in character. This also ascertains the fact that heat propagates with a finite, although quite large, velocity.

9 Conclusions

The effect of diffusion plays an important role in processing and characterization to improve material properties. The measured stress provides unique information leading to fundamental understanding of a deformation mechanism in advanced structural materials. Results indicate that the variations in magnitudes of dilatation, chemical potential, and stress are found to be a maximum near the point of application of the load. It is also observed that all the considered physical quantities vanish at a certain finite value of distance from the point of application of the load. This shows the existence of wave fronts in nonclassical thermoelasticity in contrast to those in classical thermoelasticity.

While the application of a TI produces a tensile effect on the stress, a CI leads to a compressive stress in both materials except for some initial instant of time in the case of instantaneous loading. The short-time solutions in the case of a TG show that the dilatation, stress, and chemical potential are continuous at the wave fronts due to the application of continuous and periodic loads; however, these are found to be discontinuous at the wave fronts in the case of an impulsive load in both brass and Cu materials. Moreover, in the case of a TI, all the considered functions are found to be discontinuous at the wave fronts due to continuous and periodic loads but they experience a Dirac delta singularity at the wave fronts for the case of an impulsive load.

It is observed that the thermal sources produce more variation in the profiles of the considered field functions as compared to that of mass concentration loads, because

in solids, thermal diffusion is a faster process in comparison to mass diffusion. The results of the instant study can be useful to understand the material properties under the dynamic response of various loads in the context of generalized thermoelastic diffusion.

Acknowledgment The authors are extremely thankful to the reviewer for his deep interest and valuable suggestions for the improvement of this work.

References

1. M.A. Biot, J. Appl. Phys. **27**, 240 (1956)
2. H. Lord, Y. Shulman, J. Mech. Phys. Solids **15**, 299 (1967)
3. W. Nowacki, Bull. Acad. Pol. Sci. Ser. Sci. Technol. **22**, 55 (1974)
4. W. Nowacki, Bull. Acad. Pol. Sci. Ser. Sci. Technol. **22**, 129 (1974)
5. W. Nowacki, Bull. Acad. Pol. Sci. Ser. Sci. Technol. **22**, 266 (1974)
6. W. Nowacki, Eng. Fract. Mech. **8**, 261 (1976)
7. W. Dudziak, S.J. Kowalski, Int. J. Heat Mass Transfer **32**, 2005 (1989)
8. Z.S. Olesiak, Y.A. Pyryev, Int. J. Eng. Sci. **33**, 773 (1995)
9. V.I. Danilovskaya, Prikl. Math. Mekh. **16**, 316 (1950) [in Russian]
10. V.I. Danilovskaya, Prikl. Math. Mekh. **16**, 341 (1952) [in Russian]
11. A.H. Nayfeh, Z. Angew. Math. Phys. **23**, 50 (1972)
12. Y.Q. Song, Y.C. Zhang, B.H. Lu, Int. J. Thermophys. **24**, 1 (2003)
13. H.H. Sherief, F.A. Hamza, H.A. Saleh, Int. J. Eng. Sci. **42**, 591 (2004)
14. H.H. Sherief, A.A. Helamy, J. Therm. Stress. **22**, 897 (1999)
15. H.H. Sherief, H.A. Saleh, Int. J. Solid Struct. **42**, 4484 (2005)
16. J.N. Sharma, J. Sound Vib. **301**, 979 (2007)
17. J.N. Sharma, Y.D. Sharma, P.K. Sharma, J. Sound Vib. **315**, 927 (2008)
18. N. Sharma, R. Kumar, P. Kumar, Struct. Eng. Mech. **28**, 19 (2008)
19. N. Sharma, R. Kumar, P. Kumar, Int. J. Thermophys. **29**, 1503 (2008)
20. H. Honig, U. Hirdes, J. Comput. Appl. Math. **10**, 113 (1984)
21. D.S. Chandrasekharaiah, Appl. Mech. Rev. **39**, 355 (1986)
22. W.D. Callister Jr., *Material Science and Engineering: An Introduction*, 6th edn. (Wiley India, New Delhi, 2006)
23. L.C. Thomas, *Heat Transfer* (Prentice-Hall, Upper Saddle River, 1993)